R. & M. No. 3636

MINISTRY OF TECHNOLOGY

AERONAUTICAL RESEARCH COUNCIL
REPORTS AND MEMORANDA

On Achieving Interference-Free Results from Dynamic Tests on Half-Models in Transonic Wind Tunnels

By A. W. Moore and K. C. Wight
Aerodynamics Division N.P.L.

LONDON: HER MAJESTY'S STATIONERY OFFICE
1970
PRICE 16*s* 0*d* [80*p*] NET

On Achieving Interference-Free Results from Dynamic Tests on Half-Models in Transonic Wind Tunnels

By A. W. Moore and K. C. Wight

Aerodynamics Division N.P.L.

Reports and Memoranda No. 3636*
March, 1969

Summary.

Results are presented of an experimental investigation of ventilated-wall interference on dynamic measurements using a half-model in four transonic tunnels, three of which have a slotted roof and floor whilst the other has a perforated roof and floor. In addition, the smallest slotted tunnel has alternative 'slotted-perforated' walls which have screens of variable porosity fitted behind and close to the slots. An interference-free datum is derived from tests in the other three tunnels each of which gives a ratio of model planform area to tunnel cross-sectional area of less than 0·04. It is shown that the very large dynamic interference effects in the small slotted tunnel can be reduced to small proportions with the modified slotted-perforated walls over the whole range $0{\cdot}4 \leqslant M \leqslant 1{\cdot}1$. The empirical method suggested previously for applying corrections to measurements at transonic speeds is seen to give reasonable results when only small corrections are required.

The side-wall boundary layer, in which the root of the half-wing is immersed, is shown to reduce the values of stiffness derivatives in the large tunnels by as much as 10 per cent. A simple method is suggested for correcting for boundary-layer effects on all derivatives measured with a half-model, and the corrected results are shown to be in reasonable agreement with those measured when over 80 per cent of the local boundary layer is removed by vortex generators.

CONTENTS

* Replaces N.P.L. Aero Report 1293—A.R.C. 31 049.

1. *Introduction.*

Recent advances have gone some way towards explaining the large interference effects that can occur on dynamic tests in ventilated wind tunnels[1,2]. A theoretical treatment for small wings at subsonic speeds and low frequency of oscillation was derived on the assumption that the ventilated walls behave as if they are open boundaries. Good agreement was obtained between theoretical predictions of derivatives and experimental results in NPL ventilated tunnels, but it was clear that interference persisted through the transonic speed range. Although an empirical modification to the theory gave approximate corrections at transonic speeds, it was difficult to estimate their accuracy in the absence of a reliable interference-free datum. Wall interference could be reduced by testing a small half-model in a large tunnel, but when this was done the results were significantly influenced by the side-wall boundary layer in which the root of the model was immersed.

In order to achieve an interference-free datum, further tests on a half-delta wing have now been made in which the side-wall boundary layers in the NPL 36 in × 14 in (91 cm × 36 cm) and 18 in × 14 in (46 cm × 36 cm) slotted tunnels are thinned to approximately one-fifth of their previous values by vortex generators. The results are discussed in Section 3 where a simple method for correcting for the boundary layer is suggested. In Section 4, it is shown that satisfactory interference-free derivatives can be deduced from tests in the NPL 25 in × 20 in (64 cm × 51 cm) perforated tunnel and the two slotted tunnels previously mentioned, after allowance has been made for wall interference and boundary-layer effects. Comparisons are made between the interference-free results and derivatives measured in the $9\frac{1}{2}$ in × $9\frac{1}{2}$ in (24 cm × 24 cm) slotted tunnel fitted with perforated screens behind the slots with porosity adjusted to give minimal interference[3].

2. *Equipment.*

Details of the rig for oscillating the half-model are given in Refs. 1 and 2. Only pitching-moment derivatives m_θ, $m_{\dot\theta}$ can be measured with the decaying-oscillation technique used, but, as the frequency parameter is small and measurements are made with two positions of the pitching axis, lift derivatives l_θ and $l_{\dot\theta}$ can be estimated from the following formulae:

$$l_{\theta 1} = l_{\theta 3} = \frac{m_{\theta 3} - m_{\theta 1}}{(x_3 - x_1)/\bar{c}} \tag{1}$$

$$l_{\dot\theta 1} - m_{\theta 3} = \frac{m_{\dot\theta 3} - m_{\dot\theta 1}}{(x_3 - x_1)/\bar{c}} = l_{\dot\theta 3} - m_{\theta 1} \tag{2}$$

where the equations are derived from the axis transfer relations on the assumption that, for low frequency parameters,

$$l_z = m_z = 0$$

$$l_{\dot z} = l_\theta$$

$$m_{\dot z} = m_\theta$$

and subscripts† 1, 3 refer to pitching axes $x_0 = x_1$, $x_0 = x_3$.

An essential feature of the tests is that the same rig and cropped-delta half-wing are used in four NPL ventilated tunnels—the 25 in × 20 in (64 cm × 51 cm) tunnel which has a perforated roof and floor, the 36 in × 14 in (91 cm × 36 cm) tunnel and the 18 in × 14 in (46 cm × 36 cm) tunnel which each have a slotted roof and floor, the $9\frac{1}{2}$ in × $9\frac{1}{2}$ in (24 cm × 24 cm) tunnel which can either have a slotted roof and floor or, in its modified form, a slotted roof and floor with a screen of variable porosity fitted behind the slots. The smallest tunnel gives the fairly large ratio 0·14 of model planform area to tunnel cross-sectional area whilst in the other tunnels the ratio lies between 0·02 and 0·04.

The tests were done with the rigid half-delta-model of aspect ratio $A = 2{\cdot}64$ shown in Fig. 1. A roughness band of carborundum particles near the leading edge was used to fix boundary-layer transition, and tests extended over the speed range $0{\cdot}4 \leqslant M \leqslant 1{\cdot}1$ with a natural frequency of oscillation of 53Hz.

The side-wall boundary layers in the 18 in × 14 in (46 cm × 36 cm) and 36 in × 14 in (91 cm × 36 cm) tunnels were thinned locally at the model position by vortex generators which were basically of the type suggested by Tanner *et al*[4] from measurements at low speeds. The only modifications made to allow for the higher speeds of the present tests were rounding and shortening the leading edges of the generators as shown in Fig. 2. Two pairs of generators were screwed to the tunnel wall approximately twenty boundary-layer thicknesses upstream of the model position in the pattern indicated.

3. *Side-Wall Boundary Layer.*

With the model removed from the tunnel, boundary-layer traverses were made at a station just upstream of the position of the root leading edge, and a method suggested by Garner[5] was used to estimate the boundary-layer displacement thickness. Figs. 3a and 3b show typical profiles at $M = 0{\cdot}8$ with and without vortex generators in the 18 in × 14 in (46 cm × 36 cm) tunnel and the 36 in × 14 in (91 cm ×

†Three positions of pitching axis were available but the centre axis (subscript 2 in the nomenclature of Ref. 1) has not been used in the present tests.

46 cm) tunnel respectively. Changes in Mach number in the operational speed range had negligible effect on the performance of the generators as seen in the cross plots of Fig. 4 for the former tunnel. It is clear that, where the half-model is mounted, the boundary layer is thinned to less than one-fifth of its undisturbed thickness; furthermore, rough checks showed that this very thin region extended approximately 2 in (5 cm) on either side of the centre line. This was deemed sufficient for the present purpose and no further investigation of the distribution of boundary-layer thickness was made.

Pitching-moment derivatives were measured about two pitching axes $x_0 = 0{\cdot}31\bar{c}$ and $x_0 = 1{\cdot}04\bar{c}$ with and without vortex generators on the tunnel wall, and the corresponding values of lift derivatives were estimated. The results given in Tables 1 and 2 indicate that the wall boundary layer has a considerable effect. For instance, the derivative l_θ which is equivalent to $\frac{1}{2}\, dC_L/d\alpha$ in steady flow is reduced by about 10 per cent at all speeds, and in general it is clear that the presence of the side-wall boundary layer reduces the numerical values of all the derivatives. By definition the derivatives are forces made non-dimensional with respect to the speed and density of the flow and physical dimensions of the model. It is possible that the major effect of the boundary layer is to reduce the effective size of model, i.e. the half-wing with boundary layer is equivalent to a smaller half-wing without boundary layer. This would mean that forces measured at a given speed should be divided by reduced model dimensions, and it would explain why the derivatives determined in the usual manner are apparently too small. If it is assumed that small changes in model aspect ratio have only second-order effects on the values of derivatives, it seems logical to take the equivalent model to be the half-wing with its span reduced by the tunnel boundary-layer displacement thickness. The half-wing has a span of 3·61 in (9·18 cm), root chord 3·96 in (10·06 cm) and tip chord 1·54 in (3·91 cm), so the essential dimensions of the equivalent half-wing become:

$$\text{span} = s = 3{\cdot}61 \text{ in } (9{\cdot}18 \text{ cm}) - \delta^*$$

$$\text{mean chord} = \bar{c} = 2{\cdot}75 \text{ in } (6{\cdot}98_5 \text{ cm}) - 0{\cdot}33_5\, \delta^*.$$

There is an associated small change in reduced frequency parameter $\omega\bar{c}/U$. The result of reducing the model dimensions in this way is shown in Figs. 5a to g and 6a to g where, in view of the simplicity of the method, good correlation is achieved between corrected results and values measured with the thinned boundary layer. In typical experimental configurations where $\delta^*/s \approx 0{\cdot}02$ say, the correction is small and probably negligible, but when there is a relatively-thick side-wall boundary layer, the suggested method of correction should give a significant improvement except when slender half-models are used —it is then essential to have a thin side-wall boundary layer.

4. *Results from Four Tunnels.*

4.1. *Presentation.*

In a previous report[1] attempts were made to correlate results of measurements in four NPL tunnels but the boundary-layer effect discussed in the previous section prevented the determination of a satisfactory interference-free datum. With the additional information concerning the influence of the boundary layer it is now possible to reappraise the measurements. We first determine an interference-free datum from results in the three largest tunnels obtained as follows:

(a) 36 in × 14 in (91 cm × 36 cm) slotted tunnel.

Past experience of dynamic tests in this tunnel has shown that at subsonic speeds the slotted walls behave as if they are sealed as far as wall interference is concerned, and for the half-delta-wing used in the tests the corrections for sealed walls are negligible. New liners have recently been fitted to this tunnel, but they are designed so that the tunnel is the same as before with the exception that the new liners have perforated screens fitted behind the slots. The slotted walls may not continue to behave as if they are sealed at transonic speeds, but evidence from Ref. 3 indicates that, since there are perforations fitted

behind the slots, interference should remain small at transonic speeds because negligible effects are obtained at subsonic speeds. Interference-free values for this tunnel are therefore taken to be those measured with the side-wall boundary layer thinned by vortex generators. Since no theoretical corrections for wall constraint are necessary, most weight will be given to these measurements when assessing the results from the three tunnels.

(b) 18 in × 14 in (46 cm × 36 cm) slotted tunnel.

Again from past experience it is known that the slotted walls of this tunnel do not behave as if they are completely open (as assumed in the theory of Ref. 2), but only 70 per cent of the calculated corrections for an open boundary are required. Hence, for subsonic speeds below $M = 0{\cdot}89$, interference-free values are taken to be those obtained by applying 70 per cent of the calculated corrections to results measured with a thinned boundary layer, and in accordance with the empirical suggestion in Section 4.2 of Ref. 1, the same formulae are used for $0{\cdot}89 \leqslant M \leqslant 1{\cdot}10$ with the substitution of a constant value $\beta = 0{\cdot}45$ in place of $|1-M^2|^{\frac{1}{4}}$.

(c) 25 in × 20 in (64 cm × 51 cm) perforated tunnel.

Each perforated wall behaves like an open boundary and corrections calculated direct from theory are of similar magnitude to those in the 18 in × 14 in (46 cm × 36 cm) tunnel, giving changes of order 4 per cent on stiffness and 20 per cent on damping. No measurements were made with a thin boundary layer so δ^* was estimated to be $0{\cdot}18_5$ in (0·47 cm) and corrections interpolated from the measured effect of the boundary layer on results from tunnels (a) and (b) have been applied to the stiffness derivatives. Corresponding changes in damping plotted on a scale which shows the variation of damping with Mach number were small.

The 'interference-free' derivatives from the three tunnels are shown in Figs. 7a to g and a weighted mean line, taken to be the estimated interference-free datum, is drawn in each case. In view of the uncertainty of applying corrections at transonic speeds to results measured in the 18 in × 14 in (46 cm × 36 cm) tunnel and the 25 in × 20 in (64 cm × 51 cm) tunnel, four times the weight is given to results measured in the 36 in × 14 in (91 cm × 36 cm) tunnel. Following the determination of the desired interference-free values it is of interest to examine results from the $9\frac{1}{2}$ in × $9\frac{1}{2}$ in (24 cm × 24 cm) tunnel since the original slotted walls produced very large interference effects as may be seen in Figs. 8a to g. The changes obtained at transonic speeds are also shown in order to assess the accuracy of the empirical method of correction when large interference effects are present. Derivatives measured after the tunnel had been fitted with modified walls designed to give minimal interference according to Ref. 3 are presented for the complete speed range of the tests. The free-stream theoretical curves for subsonic speeds were calculated by the method described in Ref. 6 with $(m, n, q) = (23, 3, 4)$.

4.2. *Discussion.*

A decaying-oscillation technique was employed because of the amount of information required and the number of facilities used. Although measurement of oscillatory forces in this way is relatively simple compared with inexorable forcing, some sacrifice is made in accuracy because the decaying-oscillation technique is inherently sensitive to fluctuations in tunnel flow. Furthermore the stability of the mechanical properties of the oscillating system is important, particularly in relation to the stiffness derivatives since they depend on a small change in frequency. There may also be changes in the measured derivatives due to small differences in model alignment after dismantling the apparatus and reassembling it in another tunnel, or due to changes in the condition of the roughness band. Hence, some scatter is expected in comparisons of results from the four tunnels apart from differences due to interference, and a rough assessment indicates that it is reasonable to accept a scatter of ± 3 per cent about some mean value.

It can be seen from Figs. 7a to g that the 'interference-free' values of derivatives obtained from measurements in three different tunnels are in reasonable agreement. Indeed, for the stiffness derivatives in Figs. 7a to c nearly all the results lie within 3 per cent of the weighted mean curve. The interference corrections

applied to results from the 18 in × 14 in (46 cm × 36 cm) tunnel and the 25 in × 20 in (64 cm × 51 cm) tunnel increase the numerical values of l_θ and m_θ by about 4 per cent only. Since the plotted values agree within the experimental error, the empirical corrections applied in the transonic speed range are probably of the right magnitude; for the pitching stiffness in Fig. 7c in particular, the applied corrections significantly improve the correlation of results. For the damping derivatives the empirical corrections are about 20 per cent and it is evident that consistent results are again obtained.

Figs. 8a to g show a comparison between results measured in the $9\frac{1}{2}$ in × $9\frac{1}{2}$ in (25 cm × 25 cm) tunnel and the corresponding mean interference-free curves. It is clear from Figs. 8a to c that the stiffness derivatives measured in the $9\frac{1}{2}$ in × $9\frac{1}{2}$ in (25cm × 25 cm) slotted tunnel are subject to considerable wall interference effects. When the empirical corrections at transonic speeds are applied to the pitching stiffness in Fig. 8b reasonably good results are obtained. However, when the same method is applied to pitching stiffness for the rearward pitching axis position in Fig. 8c, the corrected results are far too large. The errors are carried through to the lift derivative l_θ which is derived directly from the two pitching-moment measurements according to equation (1). However, no simple correction applied to the uncorrected lift derivative in Fig. 8a could give good agreement with the interference-free datum at transonic speeds since the trends are incompatible.

Derivatives measured in the $9\frac{1}{2}$ in × $9\frac{1}{2}$ in (25 cm × 25 cm) tunnel with walls modified by the method of Ref. 3 to give small interference on stiffness measurements (results denoted '0·31 perforations' in the figures) are seen to lie close to the interference-free datum at all speeds with the exception of the results with $M = 0{\cdot}95$. A different wall configuration is required to obtain interference-free damping derivatives and the corresponding stiffness derivatives for this condition (results denoted '0·06 perforations') are shown. The theoretical curves for unconstrained flow at subsonic speeds agree in trend but not in magnitude with the measurements.

The uncorrected damping derivatives in Figs. 8d to g are subject to very large wall-interference effects especially at the higher speeds. The measured lift derivative $l_{\dot\theta}$ in Fig. 8e for instance is about 1·0 and positive near sonic speed whereas the interference-free value is approximately 1·5 and negative. Applying corrections to $l_{\dot\theta}$ at transonic speeds does lead to an improvement but the corrected results lie only half way between the uncorrected values and the interference-free curve. The pitching damping with the rearward pitching axis is quite different in trend from the interference-free datum at transonic speeds so no simple correction could give agreement. No satisfactory explanation of the difference in trend can be offered. However, with a forward pitching axis the trends agree, but as in the case of the lift derivatives, the corrections are not large enough.

There is a dramatic reduction in wall-interference effects when the walls are modified by the method of Ref. 3 to give small interference on damping derivatives (results denoted '0·06 perforations' in the figures). The basis of the method is to adjust porosity until an interference-free damping is obtained at some convenient subsonic speed. That this derivative is then nearly interference-free at all speeds is evident in Fig. 8f, but the interference on the lift damping derivatives is not removed at any speed although it is made small. The discrepancy probably occurs because the lift damping derivatives are more sensitive to wall effects than are the pitching damping derivatives, the implication being that if wall porosity had been chosen to remove the interference on the more sensitive lift derivative, then the pitching-damping derivatives would also be free of wall constraint. There was some difficulty in measuring pitching damping at $M = 1{\cdot}00$ and $M = 1{\cdot}05$ with the rearward position of the pitching axis and an unusually large scatter was obtained (Fig. 8g). This could in part explain the apparent error in trend in this case for $M > 0{\cdot}9$. The damping derivatives which were measured when the wall condition was chosen to give interference-free stiffness are also presented. The theoretical curves for damping in unconstrained flow at subsonic speeds again agree in trend but not in magnitude with the interference-free values.

5. *Conclusions.*

1. A satisfactory interference-free datum has been obtained for a cropped-delta half-wing in the speed range $0{\cdot}4 \leqslant M \leqslant 1{\cdot}1$ from tests in three NPL ventilated tunnels whose cross-sectional areas were large relative to the area of the wing planform.

2. The empirical method suggested in Ref. 1 for correcting measurements made in ventilated tunnels at transonic speeds appears to give reasonable results when the corrections are small. However, the large corrections for the present tests in a small slotted tunnel are unreliable above $M = 0{\cdot}9$.

3. It is confirmed that large slotted-wall interference can be eliminated, as suggested in Ref. 3, by fitting suitable perforated screens behind the slots. When the NPL $9\frac{1}{2}$ in $\times$ $9\frac{1}{2}$ in (24 cm $\times$ 24 cm) slotted tunnel is modified in this way, near interference-free damping or stiffness derivatives are obtained throughout the speed range of the tunnel. However, it is not possible to remove interference on stiffness and damping simultaneously, and for reasons discussed in Ref. 3, it is in general better to aim at achieving interference-free damping derivatives if the tunnel wall condition cannot easily be varied.

4. The presence of a side-wall boundary layer can produce significant errors if small half-models are used. A simple method for correcting results measured with boundary-layer effects present is suggested, and the results after correction are usually in better agreement with values measured with the side-wall boundary layer locally thinned by vortex generators.

5. Theoretical corrections to results from dynamic tests at subsonic speeds have been extensively examined and compared with experiment in Ref. 2 where it is concluded that, although the linearized theory goes a long way towards explaining the large ventilated wall effects on dynamic measurements with models of normal size, it cannot be applied with confidence when the corrections exceed 50 per cent of measured values. The empirical method for correcting results at transonic speeds likewise becomes inaccurate. It therefore seems that there is no satisfactory way of correcting results from dynamic tests in a ventilated tunnel with large interference effects. The alternatives are to modify the geometry of the tunnel walls, as suggested in Ref. 3 for instance, or to use a small model in a large tunnel with the side-wall boundary layer thinned if a half-model technique is used. Even if a small model is used, it may still be necessary to apply corrections by the theory of Ref. 2, but these corrections should then be acceptably

6. *Acknowledgement.*

The authors wish to acknowledge the assistance of Mrs. J. A. Moreton in obtaining the large amount of experimental information presented in this report.

LIST OF SYMBOLS

A	Aspect ratio
$\bar{c}$	Mean chord of model half-wing
$\bar{C}_L$	(complex lift)/$\frac{1}{2}\rho U^2 S$
$\bar{C}_m$	(complex pitching moment)/$\frac{1}{2}\rho U^2 S\bar{c}$
M	Mach number
q	Local dynamic pressure
Q	Dynamic pressure of undisturbed stream = $\frac{1}{2}\rho U^2$
	see Figs. 3a and b
s	Span of model half-wing
S	Area of model half-wing = $s\bar{c}$
U	Velocity of undisturbed stream
x_0	Streamwise distance of pitching axis downstream of the root-chord leading edge
y	Distance from tunnel wall

z_0 Amplitude of heaving oscillation

θ_0 Amplitude of pitching oscillation

$\bar{\nu}$ Frequency parameter $= \omega\bar{c}/U$

δ^* Boundary-layer displacement thickness

ρ Density of undisturbed stream

ω Angular frequency of oscillation

Derivatives

The non-dimensional derivatives of lift l_θ, $l_{\dot{\theta}}$, l_z, $l_{\dot{z}}$ are defined by

$$\bar{C}_L = 2\theta_0(l_\theta + i\bar{\nu}l_{\dot{\theta}}) + 2\frac{zo}{\bar{c}}(l_z + i\bar{\nu}l_{\dot{z}})$$

The non-dimensional derivatives of pitching moment m_θ, $m_{\dot{\theta}}$, m_z, $m_{\dot{z}}$ are defined by

$$\bar{C}_m = 2\theta_0(m_\theta + i\bar{\nu}m_{\dot{\theta}}) + 2\frac{zo}{\bar{c}}(m_z + i\bar{\nu}m_{\dot{z}}).$$

Suffices

The suffices 1, 3 used in tabulating the results refer to the upstream axis and the downstream axis respectively.

REFERENCES

No.	*Author(s)*	*Title, etc.*
1	A. W. Moore and K. C. Wight	An experimental investigation of wall interference effects on dynamic measurements on half-models in ventilated tunnels through the transonic speed range. A.R.C. R. & M. 3570. August, 1967.
2	H. C. Garner, A. W. Moore and K. C. Wight ..	The theory of interference effects on dynamic measurements in slotted-wall tunnels at subsonic speeds and comparisons with experiment. A.R.C. R. & M. 3500. September, 1966.
3	A. W. Moore and K.C. Wight	An experimental investigation aimed at designing ventilated walls for interference-free dynamic measurements in transonic tunnels. NPL Aero Report 1307. A.R.C. 31704.
4	L. Tanner, H. H. Pearcey and Miss C. M. Tracey ..	Vortex generators; their design and their effects on turbulent boundary layers. A.R.C. 16 487. January, 1954.
5	H. C. Garner	Thickness parameters by rapid integration of turbulent boundary layers. *J. R. Aero. Soc.*, Vol. 61, pp 278–280. April, 1957.
6	H. C. Garner and D. A. Fox	Algol 60 programme for Multhopp's low-frequency subsonic-lifting-surface theory. A.R.C. R. & M. 3517. April, 1966.

TABLE 1

Derivatives Obtained for the Cropped-Delta Half-Wing in the 36 in × 14 in Tunnel

(a) Without vortex generators.

M	l_θ	$l_{\dot\theta 1}$	$l_{\dot\theta 3}$	$-m_{\theta 1}$	$m_{\theta 3}$	$-m_{\dot\theta 1}$	$-m_{\dot\theta 3}$
0·40	1·359	1·381	0·389	0·490	0·502	0·811	0·169
0·50	1·391	1·402	0·386	0·506	0·510	0·848	0·197
0·60	1·419	1·369	0·333	0·521	0·515	0·863	0·240
0·70	1·448	1·317	0·259	0·532	0·525	0·871	0·293
0·80	1·488	1·284	0·198	0·542	0·544	0·929	0·389
0·85	1·522	1·240	0·129	0·548	0·563	0·966	0·472
0·90	1·616	1·262	0·082	0·603	0·577	1·102	0·603
0·95	1·695	1·139	−0·098	0·690	0·547	1·318	0·886
1·00	1·785	0·008	−1·295	0·817	0·486	0·475	0·824
1·05	1·763	0·032	−1·255	0·824	0·463	0·496	0·811
1·10	1·791	−0·242	−1·550	0·905	0·403	0·269	0·739

(b) With vortex generators.

M	l_θ	$l_{\dot\theta 1}$	$l_{\dot\theta 3}$	$-m_{\theta 1}$	$m_{\theta 3}$	$-m_{\dot\theta 1}$	$-m_{\dot\theta 3}$
0·40	1·429	1·563	0·520	0·501	0·542	0·887	0·141
0·50	1·502	1·512	0·415	0·540	0·557	0·881	0·184
0·60	1·529	1·490	0·374	0·548	0·569	0·904	0·231
0·70	1·589	1·477	0·318	0·565	0·595	0·941	0·297
0·80	1·638	1·463	0·267	0·583	0·613	1·024	0·403
0·85	1·684	1·441	0·212	0·599	0·631	1·105	0·513
0·90	1·761	1·383	0·098	0·635	0·651	1·258	0·723
0·95	1·933	1·125	−0·286	0·819	0·592	1·386	0·997
1·00	1·916	0·035	−1·363	0·888	0·511	0·572	0·919
1·05	1·939	−0·020	−1·435	0·934	0·482	0·502	0·868
1·10	1·919	−0·481	−1·881	0·952	0·448	0·144	0·822

TABLE 2

Derivatives Obtained for the Cropped-Delta Half-Wing in the 18 *in* × 14 *in Tunnel*

(a) Without vortex generators.

M	l_θ	$l_{\dot\theta 1}$	$l_{\dot\theta 3}$	$-m_{\theta 1}$	$m_{\theta 3}$	$-m_{\dot\theta 1}$	$-m_{\dot\theta 3}$
0·40	1·343	1·531	0·550	0·475	0·505	0·870	0·121
0·50	1·358	1·479	0·488	0·489	0·503	0·846	0·133
0·60	1·395	1·524	0·506	0·499	0·519	0·900	0·166
0·70	1·436	1·517	0·469	0·516	0·533	0·940	0·221
0·80	1·483	1·450	0·367	0·531	0·552	0·973	0·318
0·85	1·538	1·525	0·402	0·555	0·568	1·071	0·373
0·90	1·620	1·495	0·312	0·595	0·588	1·158	0·496
0·95	1·826	1·338	0·005	0·768	0·565	1·332	0·768
1·00	1·841	0·076	−1·269	0·836	0·508	0·537	0·852
1·05	1·852	0·177	−1·175	0·914	0·439	0·602	0·793
1·10	1·829	−0·309	−1·644	0·930	0·405	0·227	0·748

(b) With vortex generators.

M	l_θ	$l_{\dot\theta 1}$	$l_{\dot\theta 3}$	$-m_{\theta 1}$	$m_{\theta 3}$	$-m_{\dot\theta 1}$	$-m_{\dot\theta 3}$
0·40	1·467	1·561	0·490	0·535	0·536	0·861	0·112
0·50	1·489	1·606	0·518	0·552	0·535	0·909	0·127
0·60	1·505	1·566	0·468	0·557	0·542	0·916	0·168
0·70	1·644	1·639	0·439	0·620	0·580	1·002	0·230
0·80	1·702	1·543	0·301	0·637	0·606	1·025	0·341
0·85	1·709	1·536	0·288	0·636	0·612	1·077	0·403
0·90	1·790	1·651	0·344	0·679	0·628	1·306	0·560
0·95	1·953	1·171	−0·255	0·849	0·577	1·307	0·874
1·00	1·919	1·101	−1·300	0·886	0·515	0·592	0·894
1·05	1·926	0·083	−1·322	0·963	0·442	0·584	0·846
1·10	1·869	−0·424	−1·788	0·961	0·403	0·129	0·733

TABLE 3

Derivatives Corrected for Wall Interference for the Cropped-Delta Half-Wing in the 18 in × 14 in Tunnel with Vortex Generators

M	l_θ	$l_{\dot\theta 1}$	$l_{\dot\theta 3}$	$-m_{\theta 1}$	$m_{\theta 3}$	$-m_{\dot\theta 1}$	$-m_{\dot\theta 3}$
0·40	1·499	1·465	0·371	0·548	0·547	0·826	0·153
0·50	1·523	1·500	0·389	0·563	0·546	0·868	0·171
0·60	1·540	1·344	0·322	0·571	0·553	0·872	0·218
0·70	1·683	1·471	0·239	0·637	0·594	0·940	0·297
0·80	1·749	1·315	0·037	0·656	0·620	0·941	0·431
0·85	1·758	1·268	−0·015	0·657	0·626	0·980	0·508
0·90	1·846	1·293	−0·056	0·704	0·643	1·176	0·699
0·95	2·013	0·649	−0·825	0·877	0·592	1·096	1·051
1·00	1·968	0·714	−1·749	0·908	0·529	0·414	1·028
1·05	1·975	−0·333	−1·774	0·988	0·459	0·389	0·964
1·10	1·915	−0·827	−2·226	0·985	0·417	−0·070	0·836

TABLE 4

Derivatives Corrected for Wall Interference for the Cropped-Delta Half-Wing in the 25 in × 20 in Tunnel with Boundary-Layer Allowance

M	l_θ	$l_{\dot\theta 1}$	$l_{\dot\theta 3}$	$-m_{\theta 1}$	$m_{\theta 3}$	$-m_{\dot\theta 1}$	$-m_{\dot\theta 3}$
0·40	1·438	1·419	0·456	0·505	0·539	0·836	0·168
0·50	1·530	1·391	0·364	0·541	0·568	0·851	0·221
0·60	1·560	1·357	0·312	0·551	0·580	0·865	0·268
0·66	1·591	1·321	0·248	0·564	0·590	0·878	0·315
0·80	1·696	1·229	0·093	0·606	0·624	0·941	0·466
0·87	1·768	1·272	0·087	0·632	0·654	1·053	0·558
0·95	2·005	1·133	−0·230	0·827	0·628	1·349	0·950
1·00	2·070	−0·170	−1·570	0·950	0·551	0·399	0·900
1·05	2·048	−0·261	−1·615	0·999	0·508	0·389	0·886

TABLE 5

Measured Derivatives for the Cropped-Delta Half-Wing in the $9\frac{1}{2}$ in × $9\frac{1}{2}$ in Tunnel with Slotted-Perforated Walls

(a) With 0·06 in perforations.

M	l_θ	$l_{\dot\theta 1}$	$l_{\dot\theta 3}$	$-m_{\theta 1}$	$m_{\theta 3}$	$-m_{\dot\theta 1}$	$-m_{\dot\theta 3}$
0·40	1·616	1·622	0·491	0·593	0·602	0·900	0·132
0·50	1·631	1·591	0·449	0·601	0·606	0·909	0·166
0·60	1·680	1·576	0·400	0·615	0·628	0·927	0·210
0·70	1·732	1·564	0·352	0·633	0·648	0·964	0·270
0·80	1·793	1·539	0·284	0·657	0·669	1·035	0·374
0·85	1·812	1·538	0·270	0·666	0·674	1·110	0·453
0·90	1·887	1·554	0·233	0·722	0·674	1·255	0·586
0·95	1·955	1·449	0·081	0·827	0·619	1·350	0·720
1·00	1·975	0·654	−0·729	0·909	0·522	0·890	0·794
1·05	2·005	0·134	−1·269	0·972	0·511	0·580	0·835

(b) With 0·31 in perforations.

M	l_θ	$l_{\dot\theta 1}$	$l_{\dot\theta 3}$	$-m_{\theta 1}$	$m_{\theta 3}$	$-m_{\dot\theta 1}$	$-m_{\dot\theta 3}$
0·40	1·472	1·764	0·734	0·523	0·565	0·970	0·073
0·50	1·506	1·735	0·681	0·533	0·581	0·970	0·105
0·60	1·560	1·704	0·612	0·555	0·599	0·974	0·144
0·70	1·624	1·689	0·552	0·586	0·616	0·999	0·192
0·80	1·695	1·759	0·573	0·619	0·634	1·106	0·260
0·85	1·727	1·822	0·613	0·629	0·649	1·198	0·316
0·90	1·750	1·856	0·631	0·635	0·660	1·334	0·435
0·95	1·829	1·813	0·533	0·740	0·613	1·520	0·620
1·00	1·923	1·106	−0·240	0·856	0·567	1·150	0·734
1·05	1·972	0·623	−0·757	0·937	0·522	0·834	0·740

TABLE 6

Theoretical Free-Stream Values of Derivatives for the Cropped-Delta Half-Wing

M	l_θ	$l_{\dot\theta 1}$	$l_{\dot\theta 3}$	$-m_{\theta 1}$	$m_{\theta 3}$	$-m_{\dot\theta 1}$	$-m_{\dot\theta 3}$
0·40	1·5256	1·6180	0·5120	0·4891	0·6170	0·9462	0·2205
0·50	1·5581	1·6352	0·5056	0·4990	0·6308	0·9831	0·2549
0·60	1·6022	1·6588	0·4972	0·5122	0·5960	1·0374	0·3057
0·70	1·6637	1·6923	0·4864	0·5304	0·6758	1·1227	0·3858
0·80	1·7425	1·7376	0·4743	0·5530	0·7103	1·2692	0·5244
0·87	1·7916	1·7711	0·4725	0·5651	0·7340	1·4470	0·7144

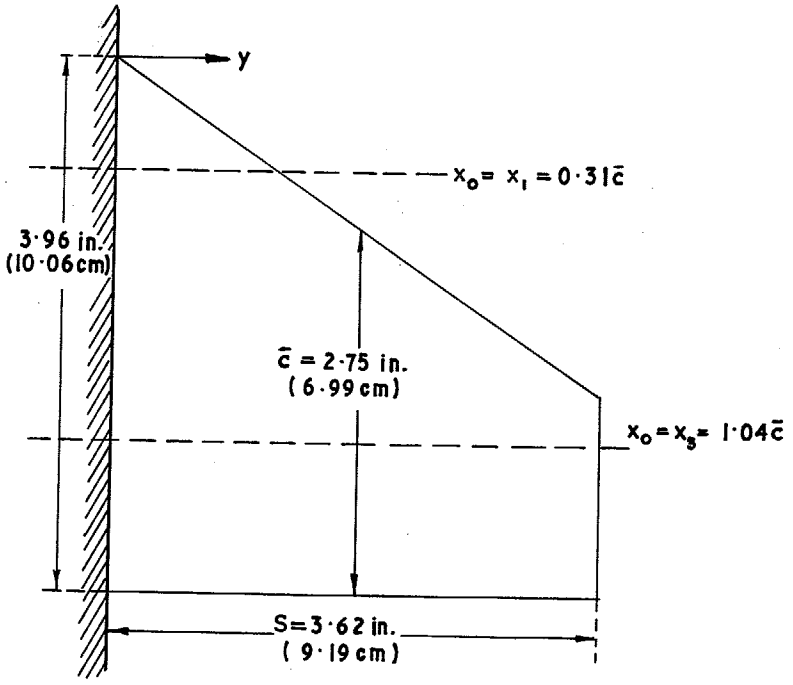

FIG. 1. Planform of cropped-delta half-wing, $A = 2{\cdot}64$, showing positions of pitching axes.

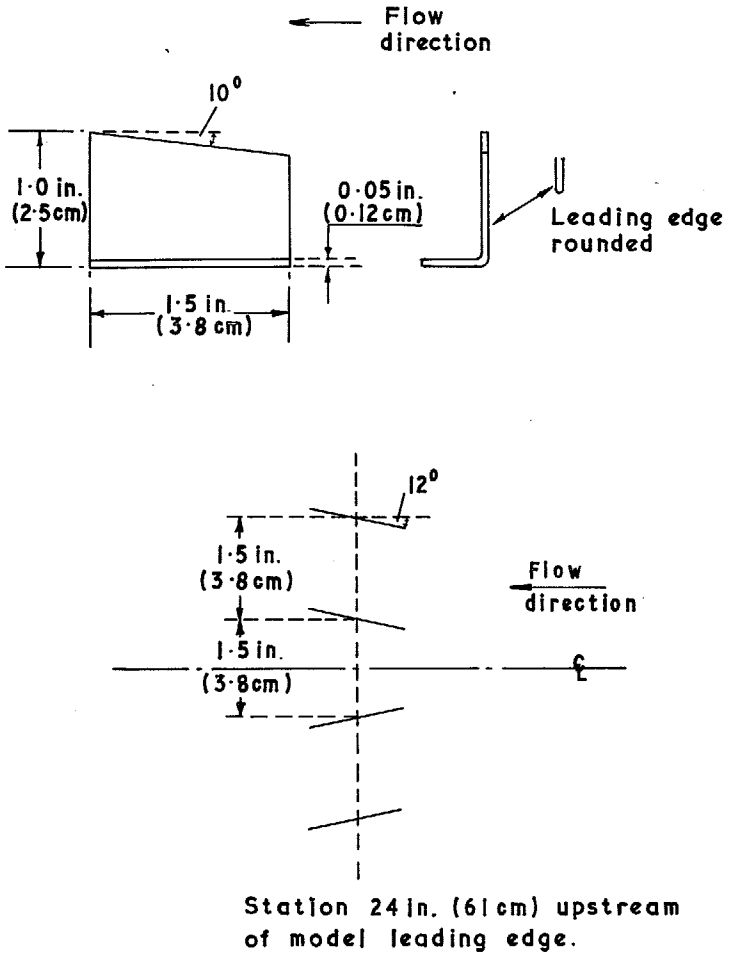

FIG. 2. The vortex generators used to thin the tunnel side-wall boundary layer.

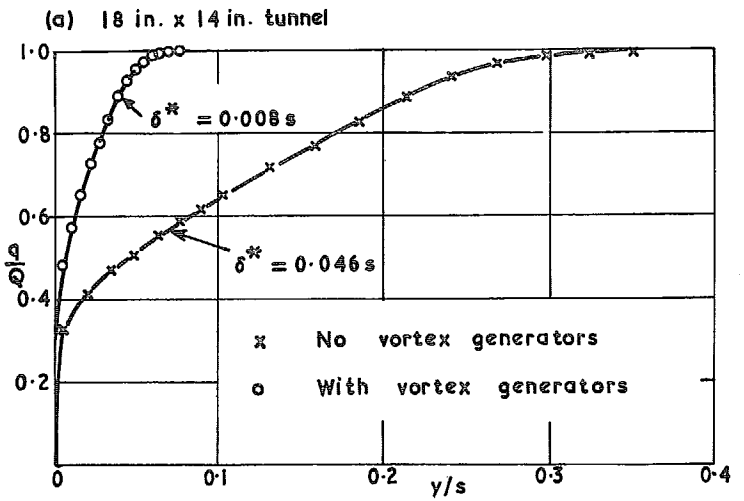

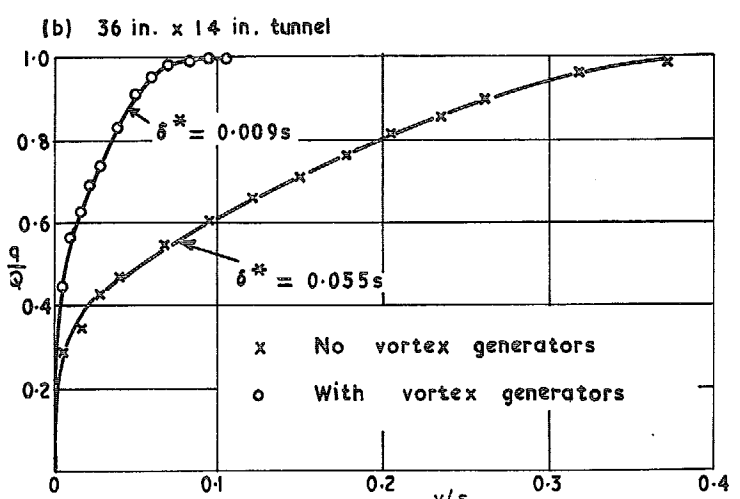

FIG. 3. Boundary layer profiles in the 18 in × 14 in and 36 in × 14 in tunnels with and without vortex generators at $M = 0{\cdot}8$.

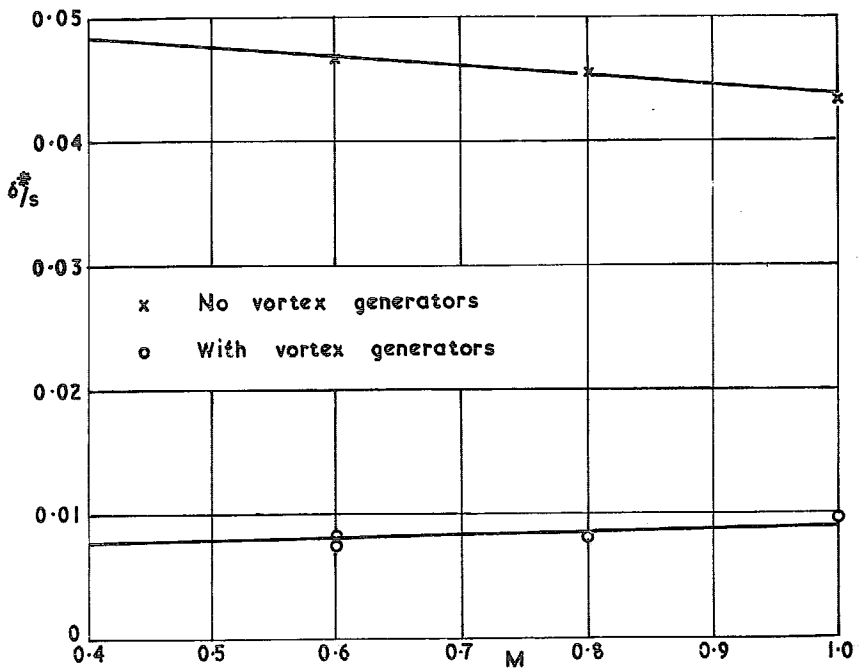

FIG. 4. The effect of vortex generators on the side-wall boundary layer at the centreline of the NPL 18 in × 14 in tunnel.

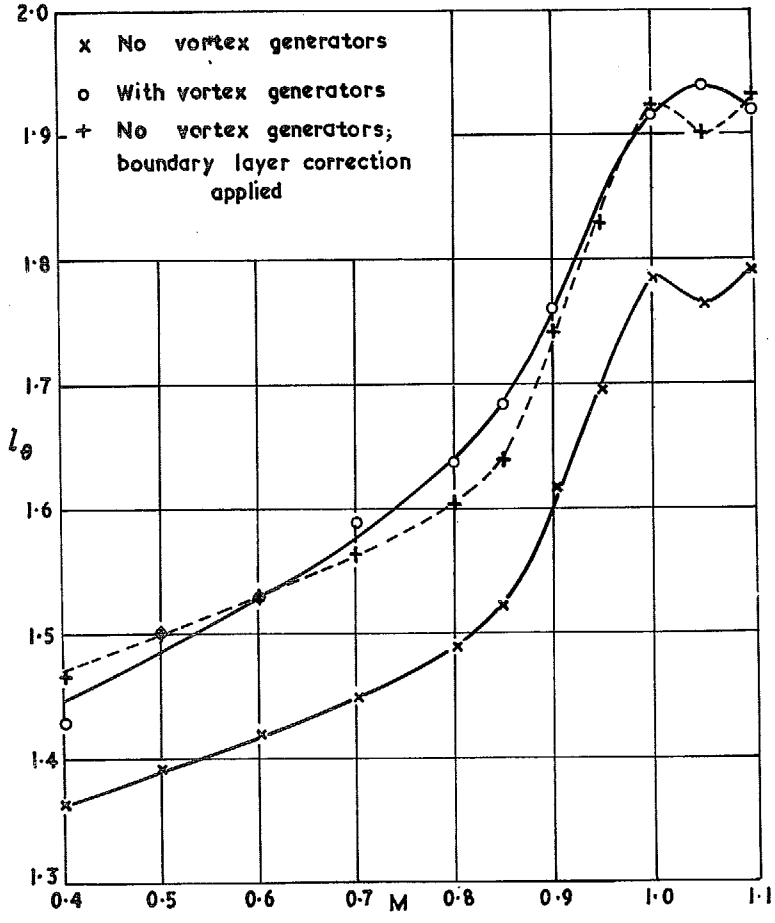

FIG. 5a. Lift derivative l_θ against Mach number, showing the effect of thinning the side-wall boundary layer in the 36 in × 14 in tunnel.

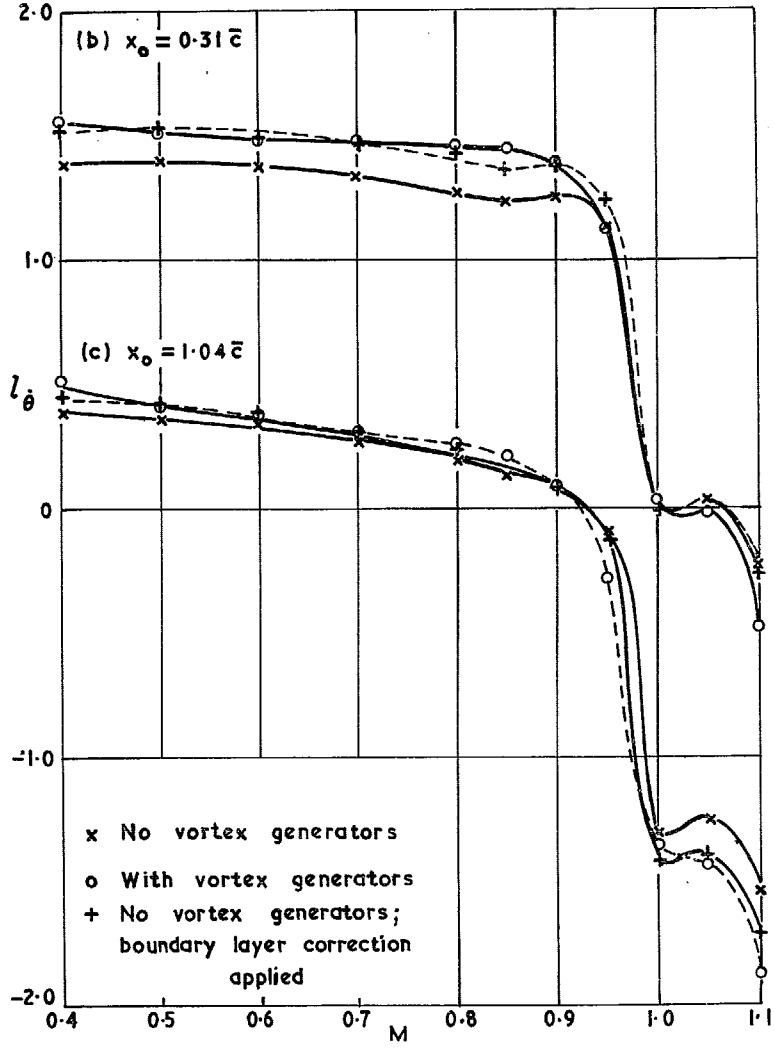

FIGS. 5b & c. Lift derivative $l_{\dot\theta}$ against Mach number, showing the effect of thinning the side-wall boundary layer in the 36 in × 14 in tunnel.

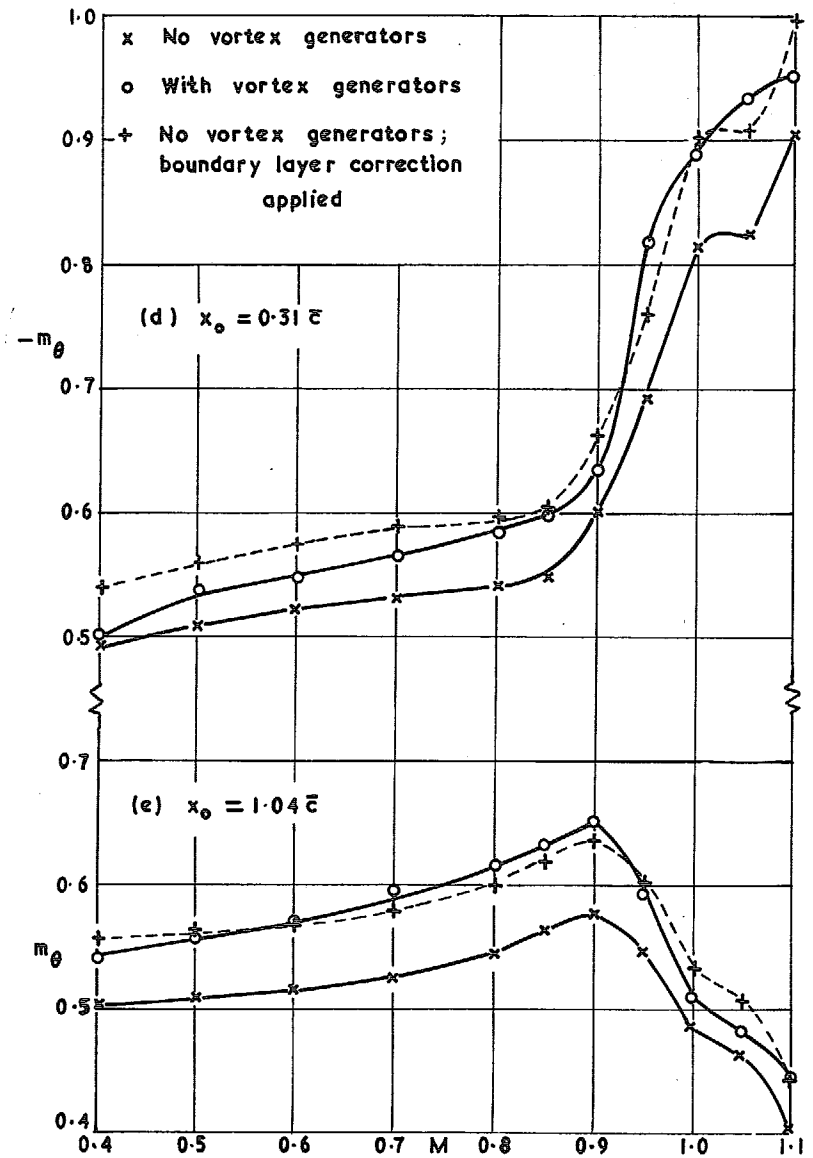

FIGS. 5d & e. Pitching stiffness against Mach number, showing the effect of thinning the side-wall

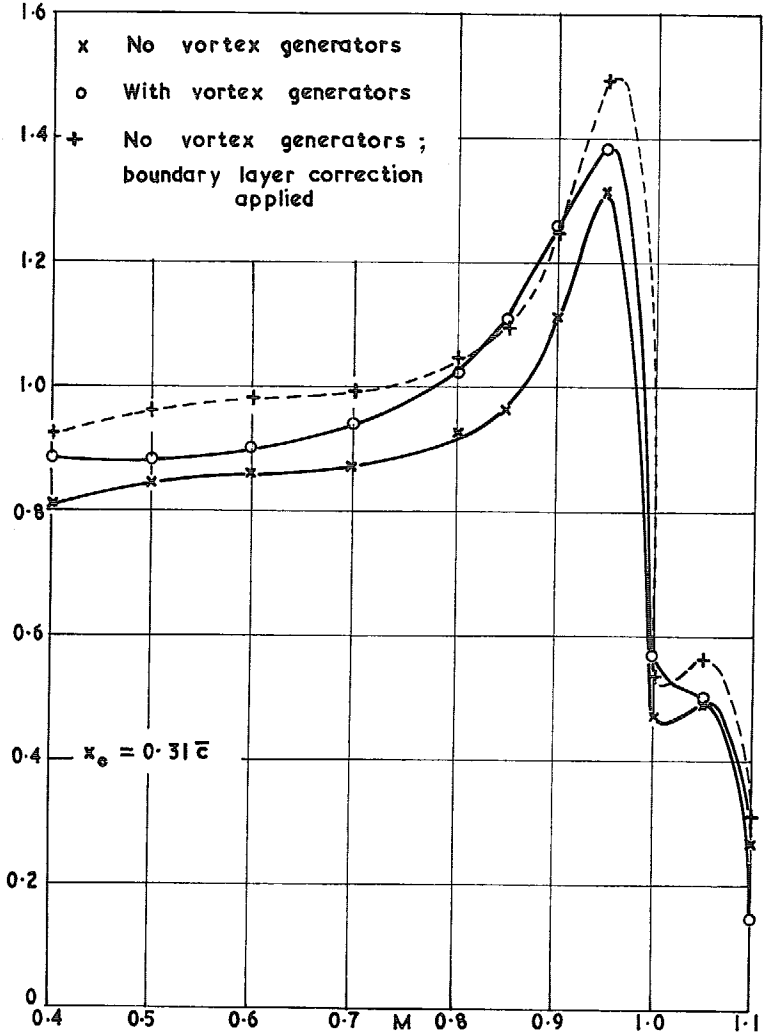

FIG. 5f. Pitching damping against Mach number, showing the effect of thinning the side-wall boundary layer in the 36 in × 14 in tunnel.

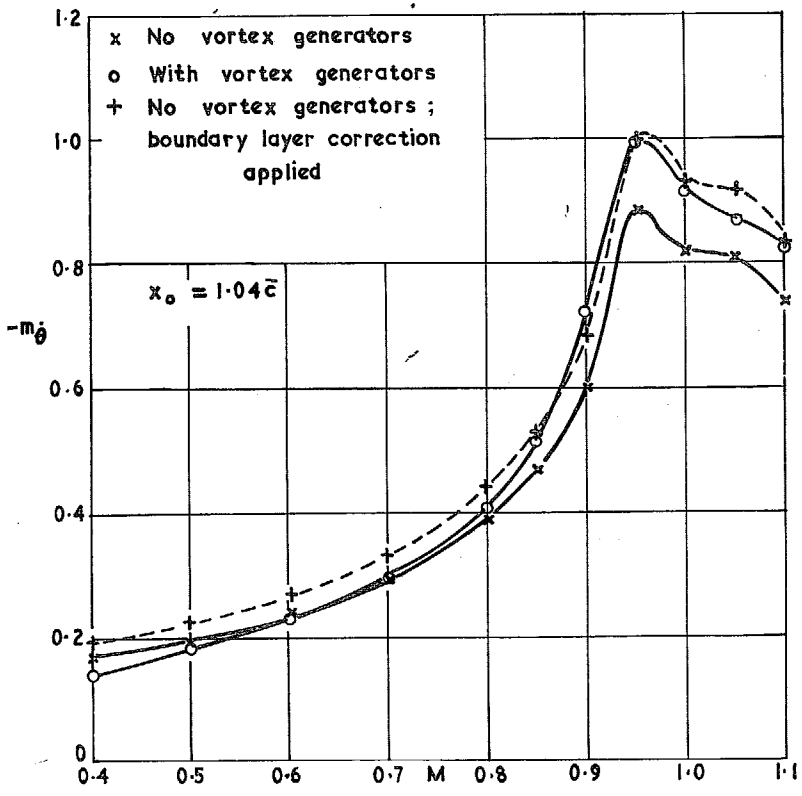

FIG. 5g. Pitching damping against Mach number, showing the effect of thinning the side-wall boundary layer in the 36 in × 14 in tunnel.

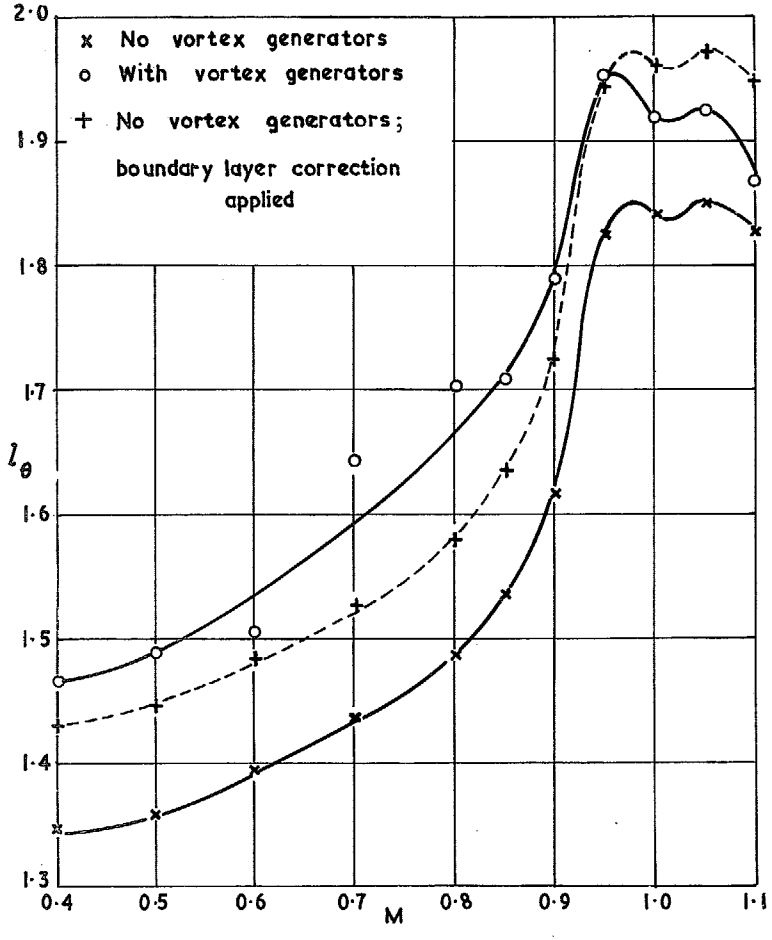

FIG. 6a. Lift derivative l_θ against Mach number, showing the effect of thinning the side-wall boundary layer in the 18 in × 14 in tunnel.

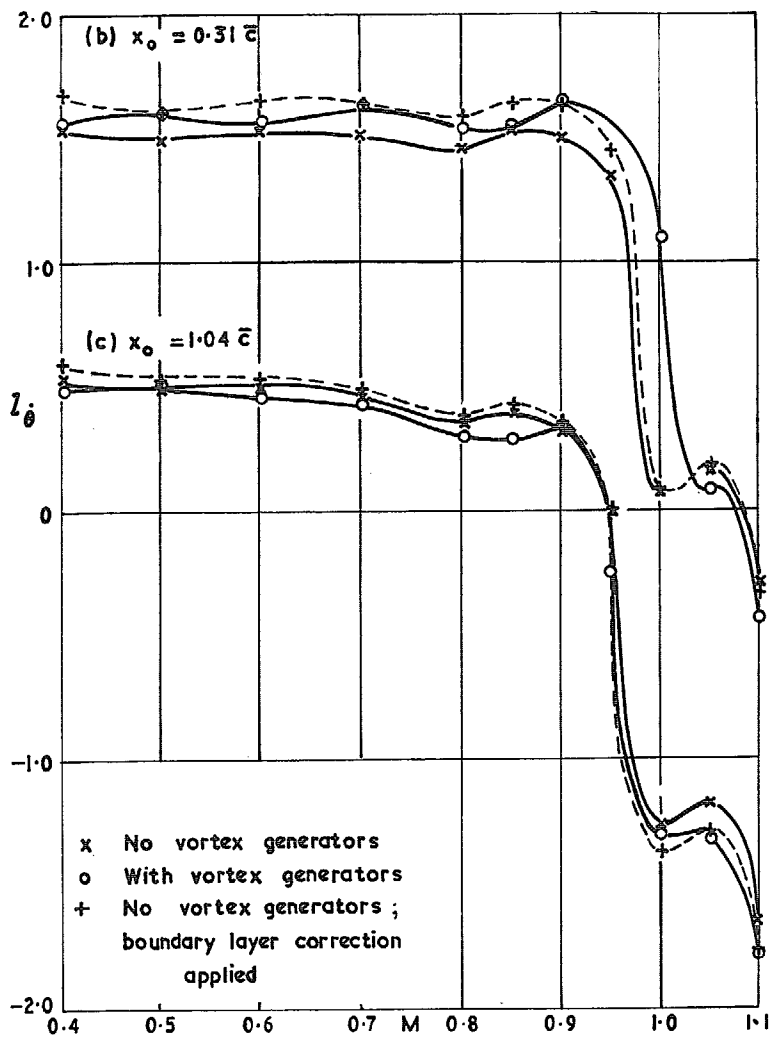

FIG. 6b & c. Lift derivative $l_{\dot{\theta}}$ against Mach number, showing the effect of thinning the side-wall boundary layer in the 18 in × 14 in tunnel.

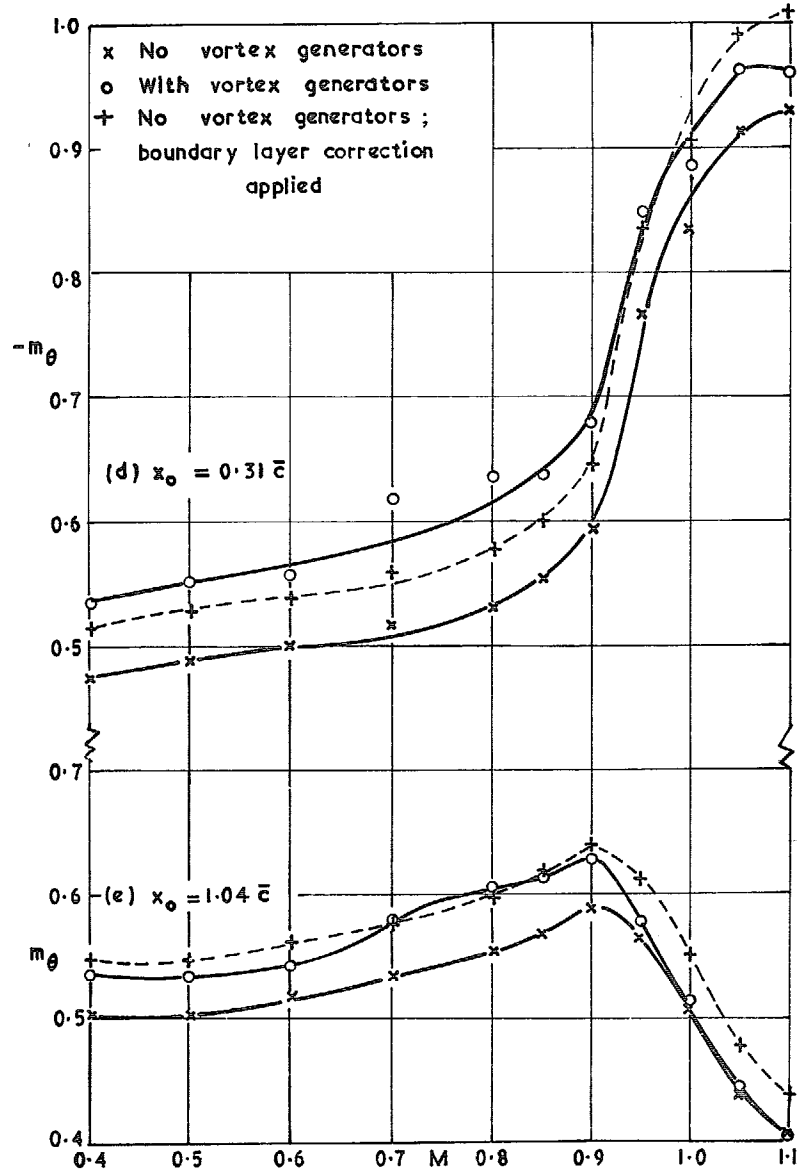

FIGS. 6d & e. Pitching stiffness against Mach number, showing the effect of thinning the side-wall

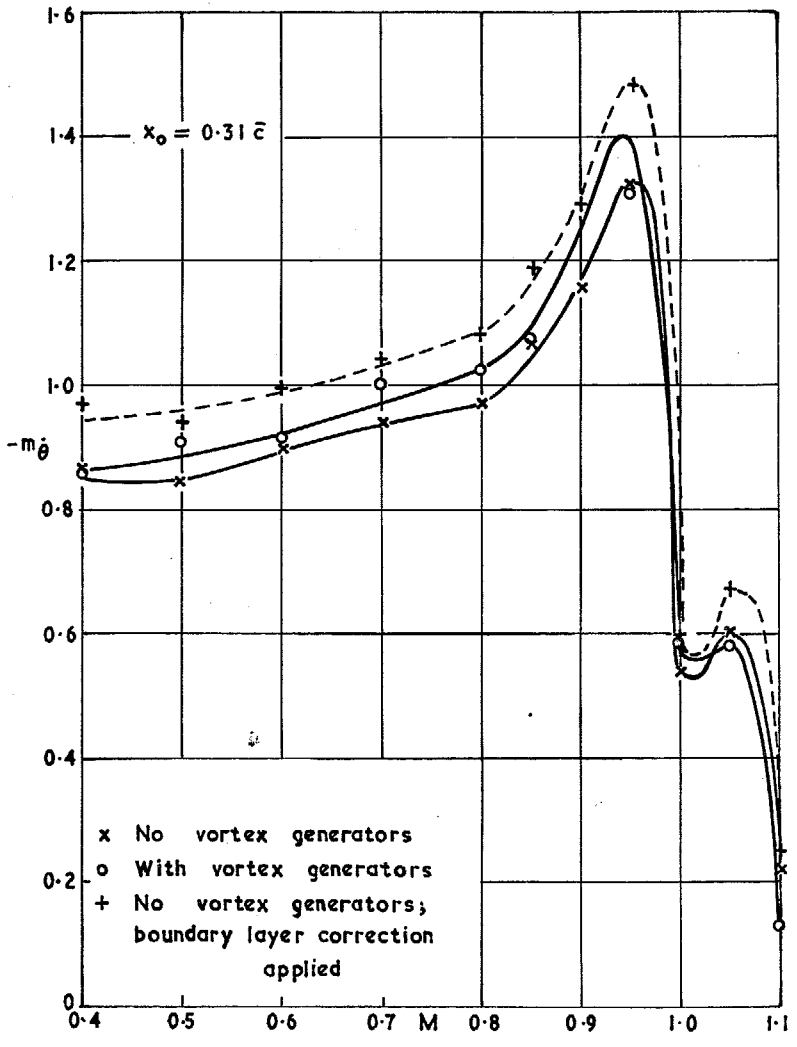

FIG. 6f. Pitching damping against Mach number, showing the effect of thinning the side-wall boundary layer in the 18 in × 14 in tunnel.

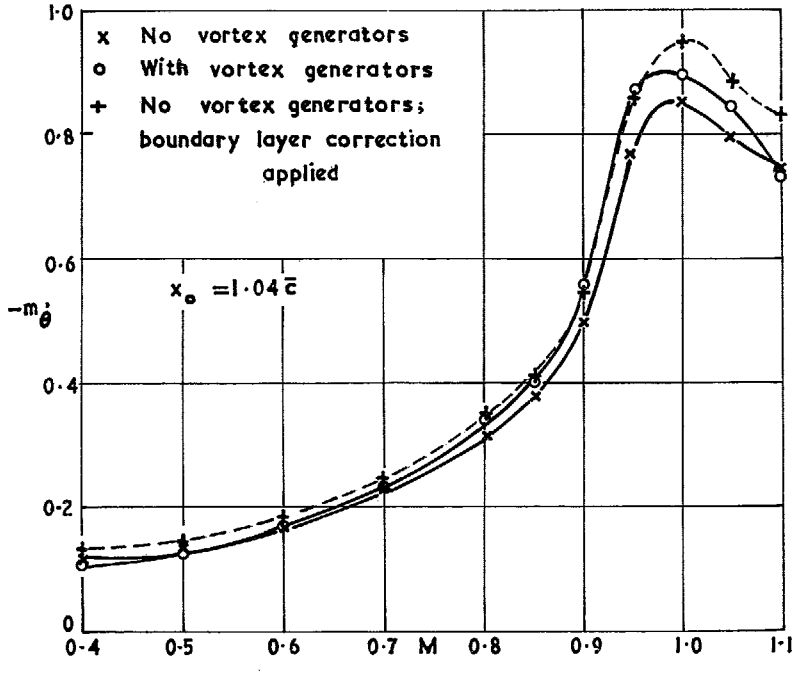

FIG. 6g. Pitching damping against Mach number, showing the effect of thinning the side-wall boundary layer in the 18 in × 14 in tunnel.

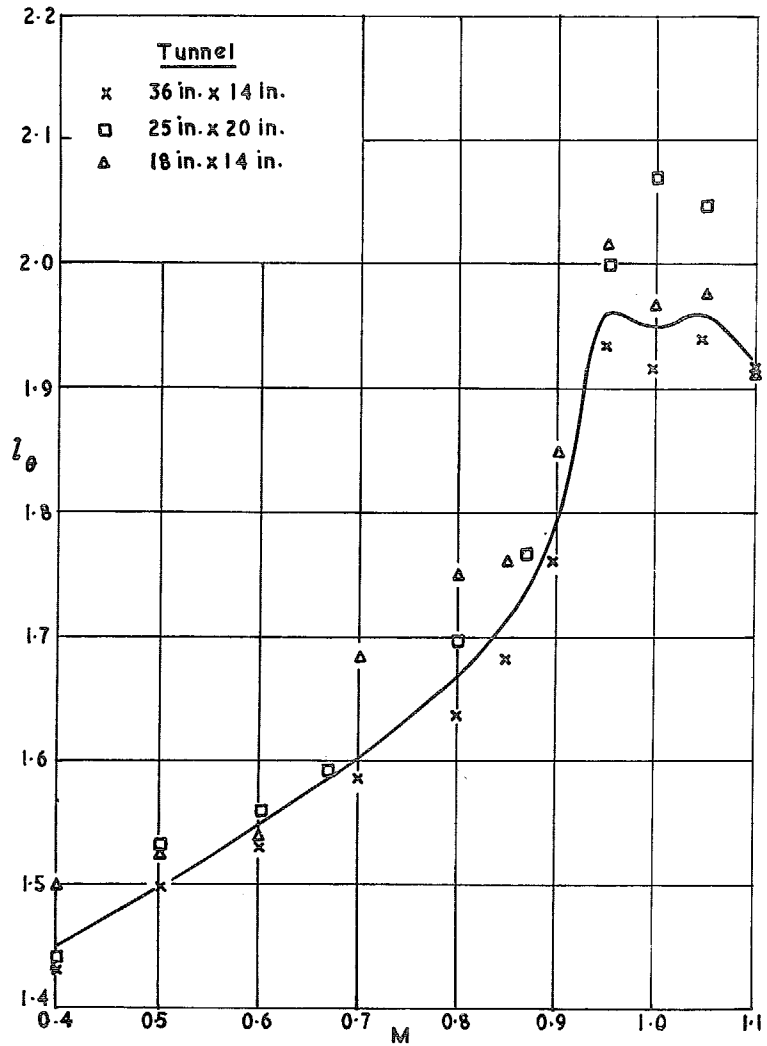

FIG. 7a. Lift derivative l_θ against Mach number, showing corrected results from measurements on a half-delta wing in three NPL ventilated tunnels.

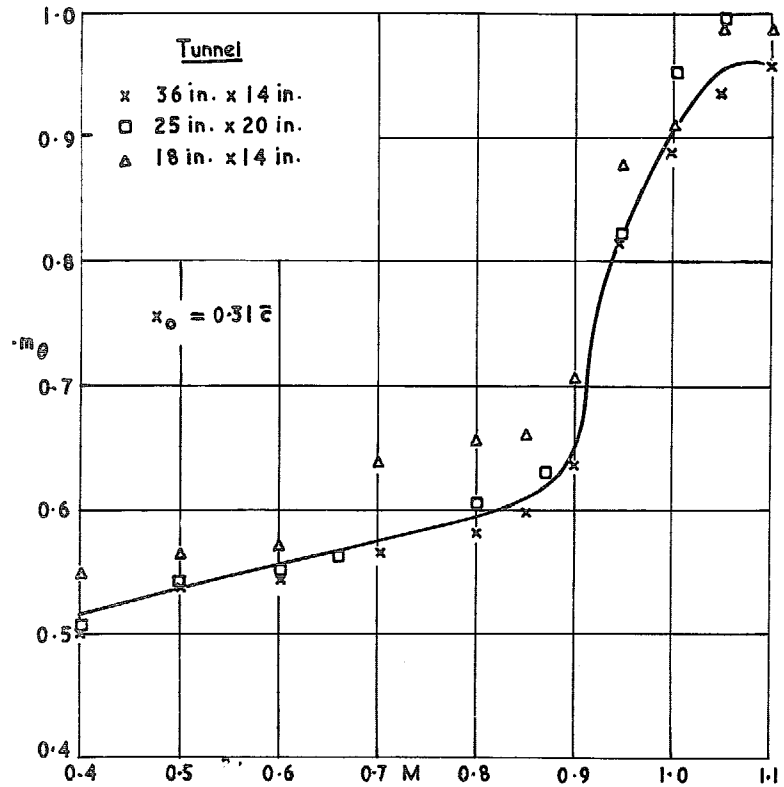

FIG. 7b. Pitching stiffness against Mach number, showing corrected results from measurements on a half-delta wing in three NPL ventilated tunnels.

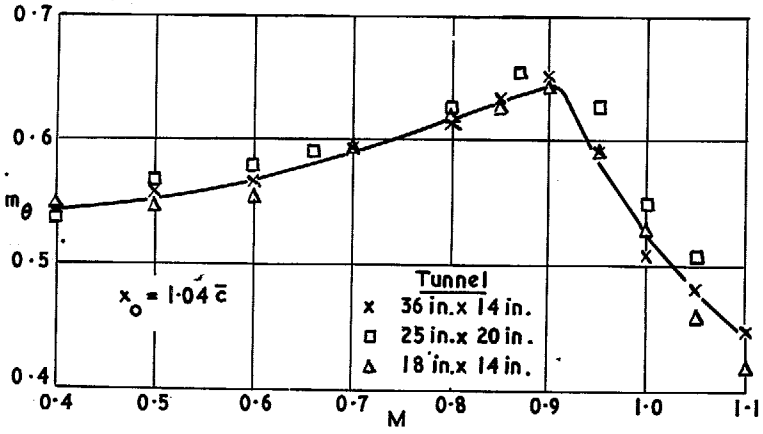

FIG. 7c. Pitching stiffness against Mach number, showing corrected results from measurements on a half-delta wing in three NPL ventilated tunnels.

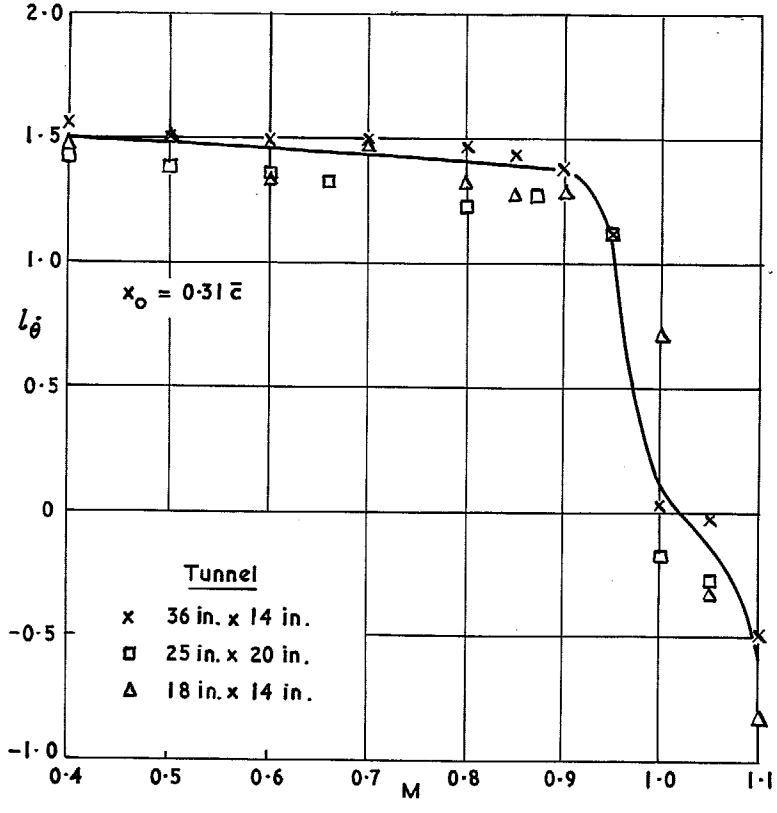

FIG. 7d. Lift derivative $l_{\dot\theta}$ against Mach number, showing corrected results from measurements on a half-delta wing in three NPL ventilated tunnels.

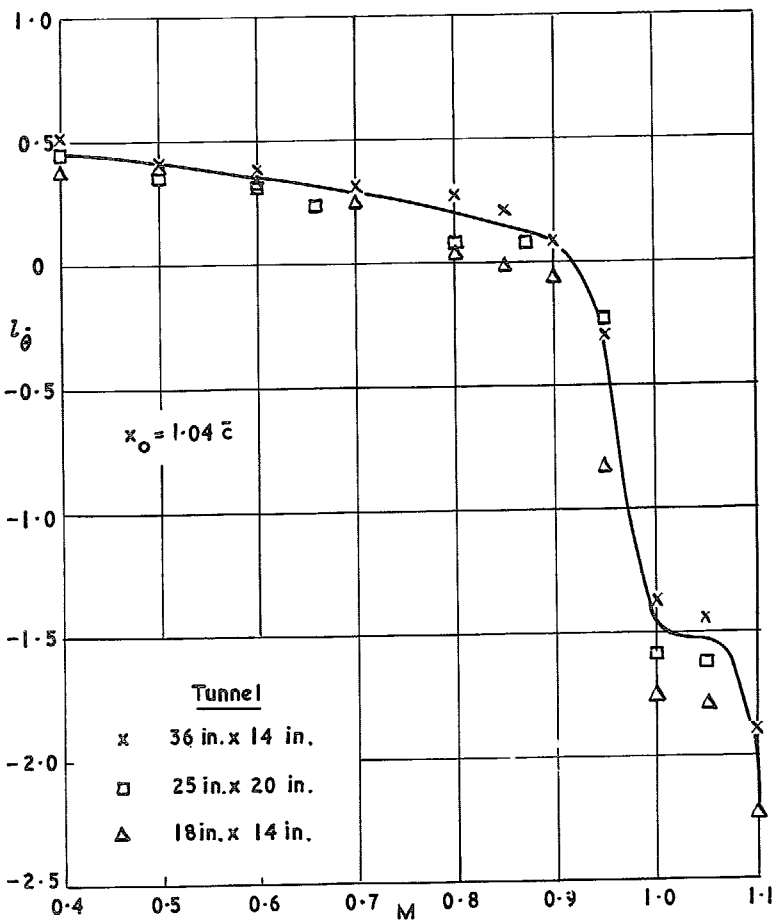

FIG. 7e. Lift derivative $l_{\dot{\theta}}$ against Mach number, showing corrected results from measurements on a half-delta wing in three NPL ventilated tunnels.

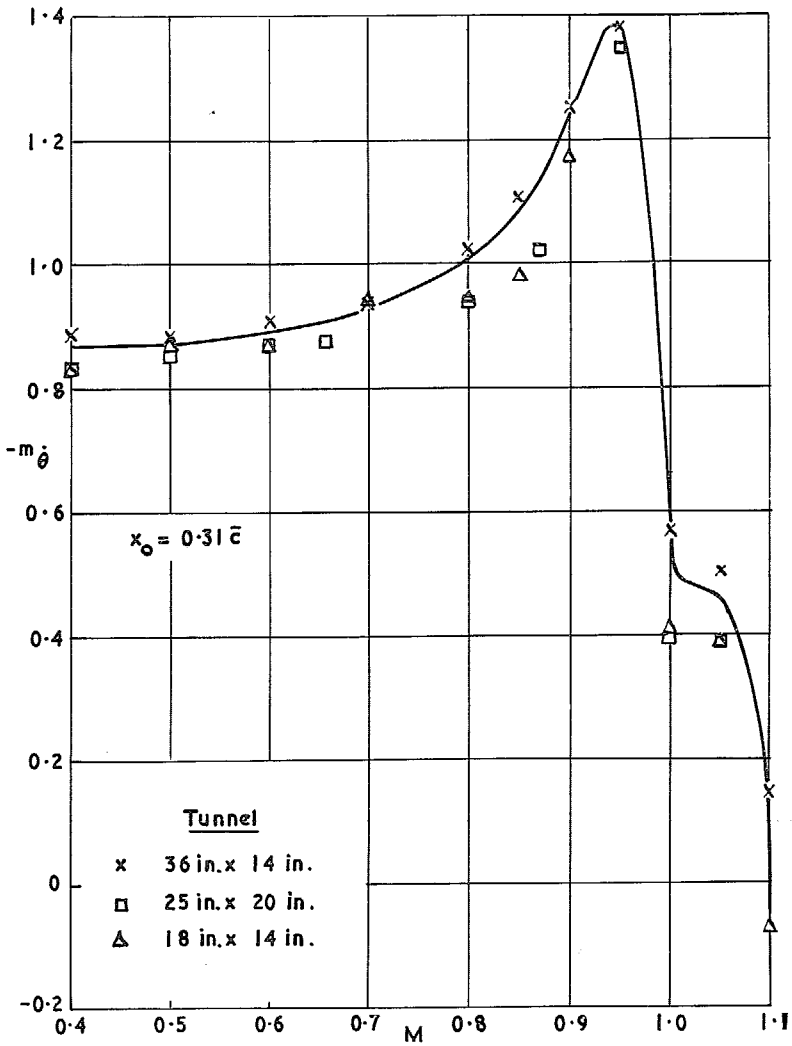

FIG. 7f. Pitching damping against Mach number, showing corrected results from measurements on a half-delta wing in three NPL ventilated tunnels.

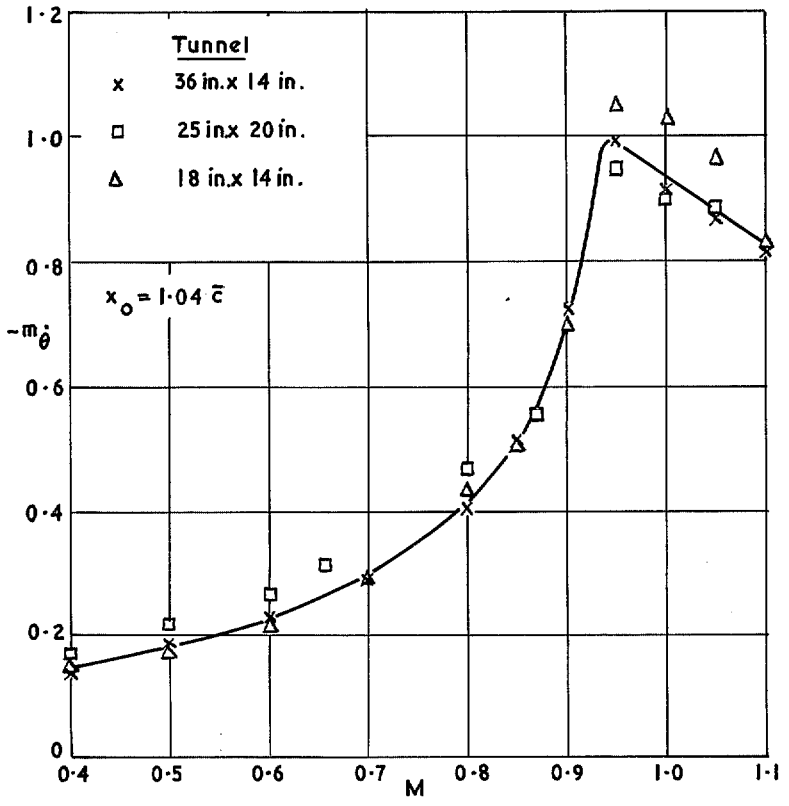

FIG. 7g. Pitching damping against Mach number, showing corrected results from measurements on a half-delta wing in three NPL ventilated tunnels.

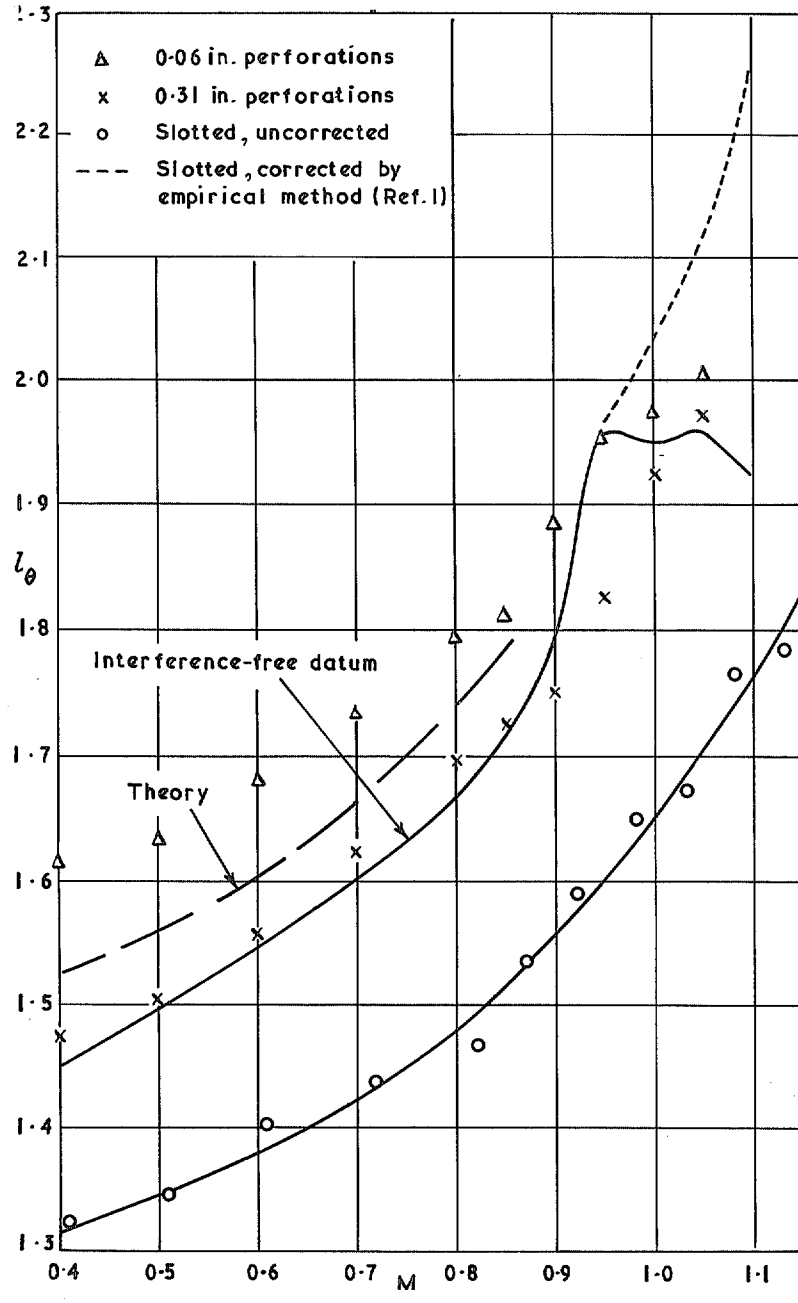

FIG. 8a. Comparison of results from the $9\frac{1}{2}$ in × $9\frac{1}{2}$ in tunnel with interference-free values of lift derivative l_θ.

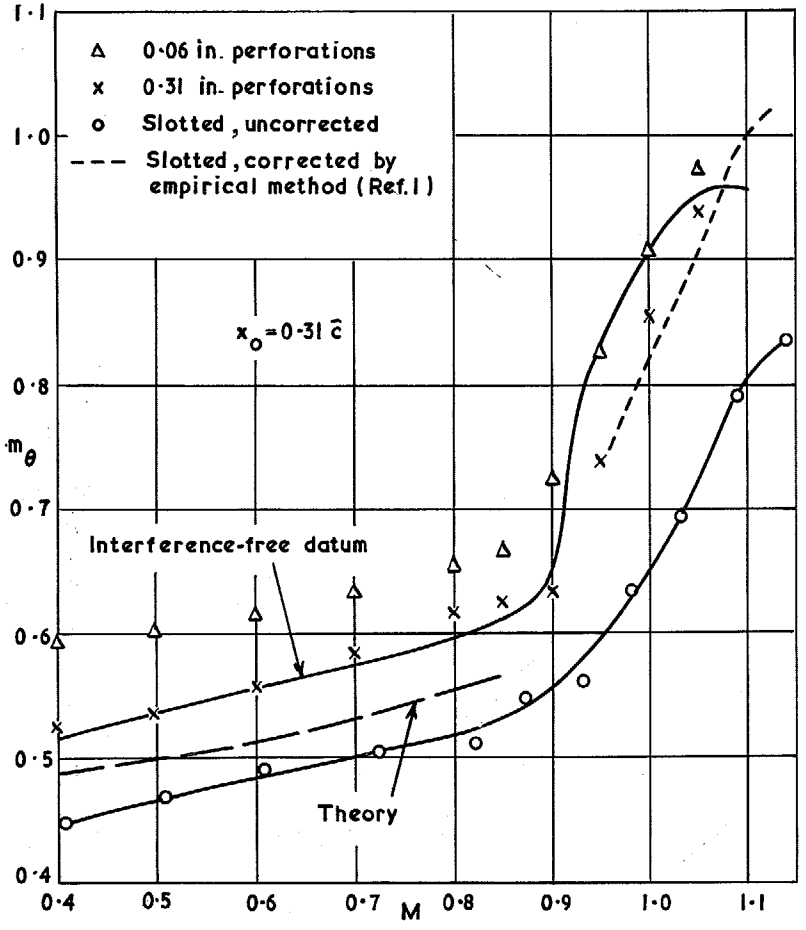

FIG. 8b. Comparison of results from the $9\frac{1}{2}$ in × $9\frac{1}{2}$ in tunnel with interference-free values of pitching stiffness.

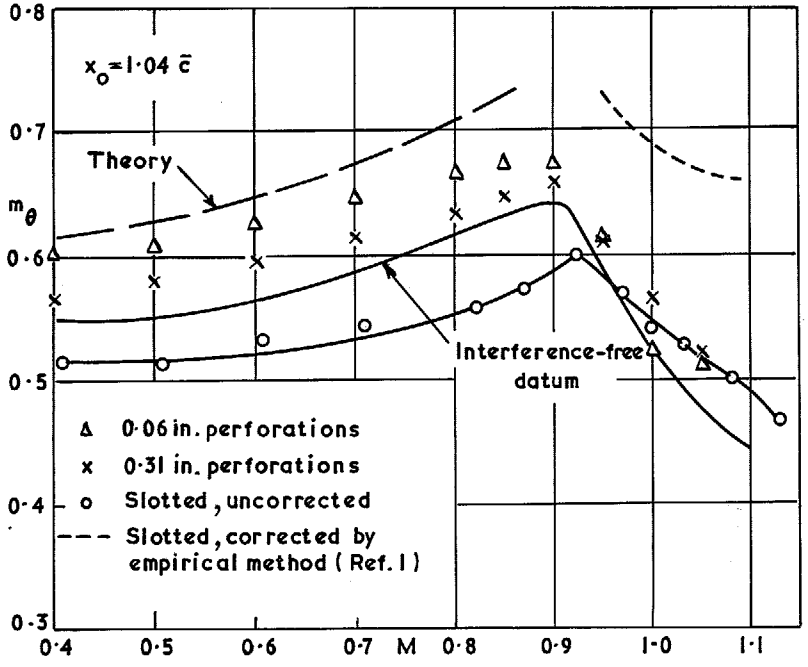

FIG. 8c. Comparison of results from the $9\frac{1}{2}$ in × $9\frac{1}{2}$ in tunnel with interference-free values of pitching stiffness.

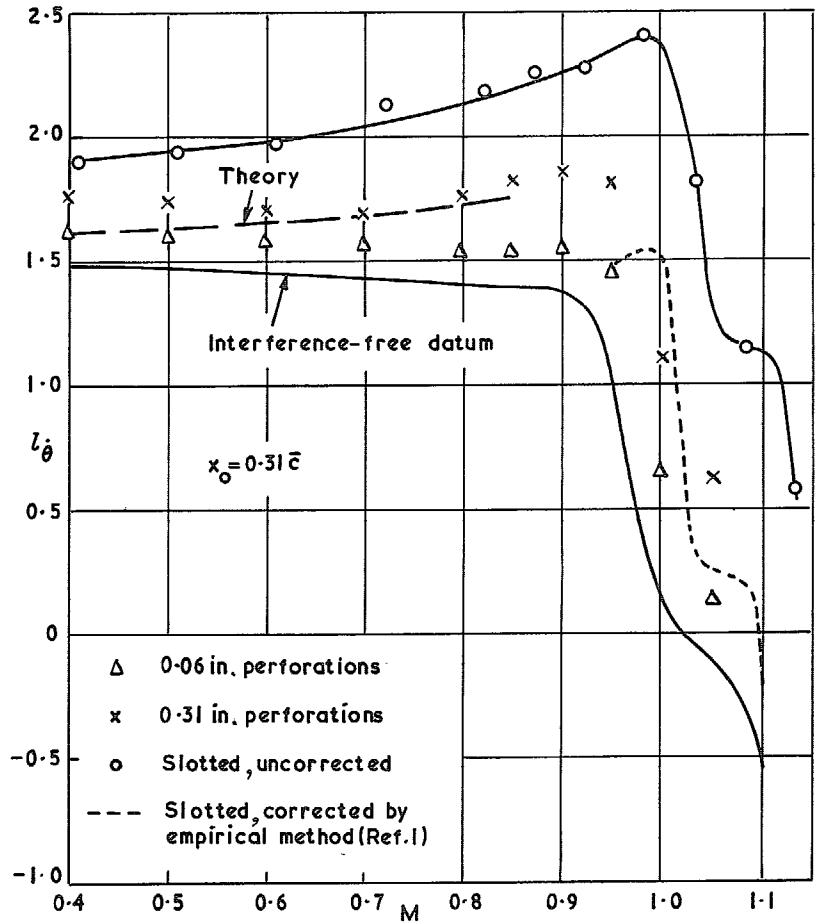

FIG. 8d. Comparison of results from the $9\frac{1}{2}$ in × $9\frac{1}{2}$ in tunnel with interference-free values of lift derivative $l_{\dot{\theta}}$.

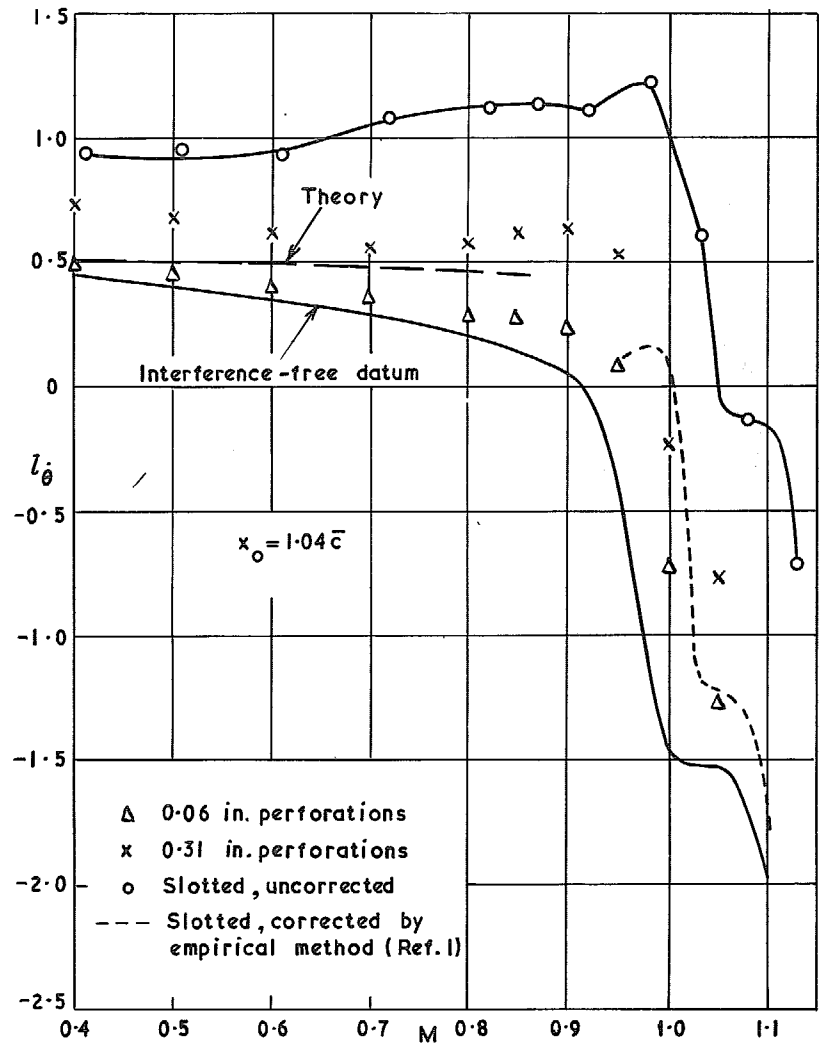

FIG. 8e. Comparison of results from the $9\frac{1}{2}$ in × $9\frac{1}{2}$ in tunnel with interference-free values of lift derivative $l_{\dot{\theta}}$.

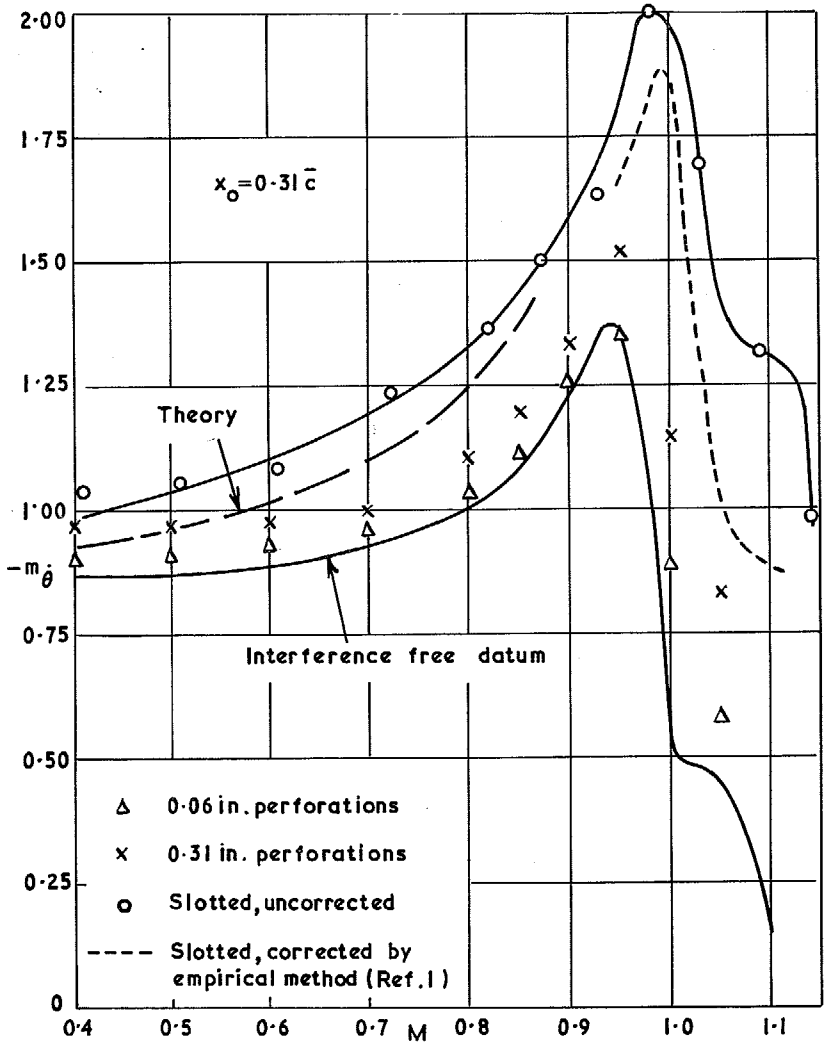

FIG. 8f. Comparison of results from the $9\frac{1}{2}$ in × $9\frac{1}{2}$ in tunnel with interference-free values of pitching damping.

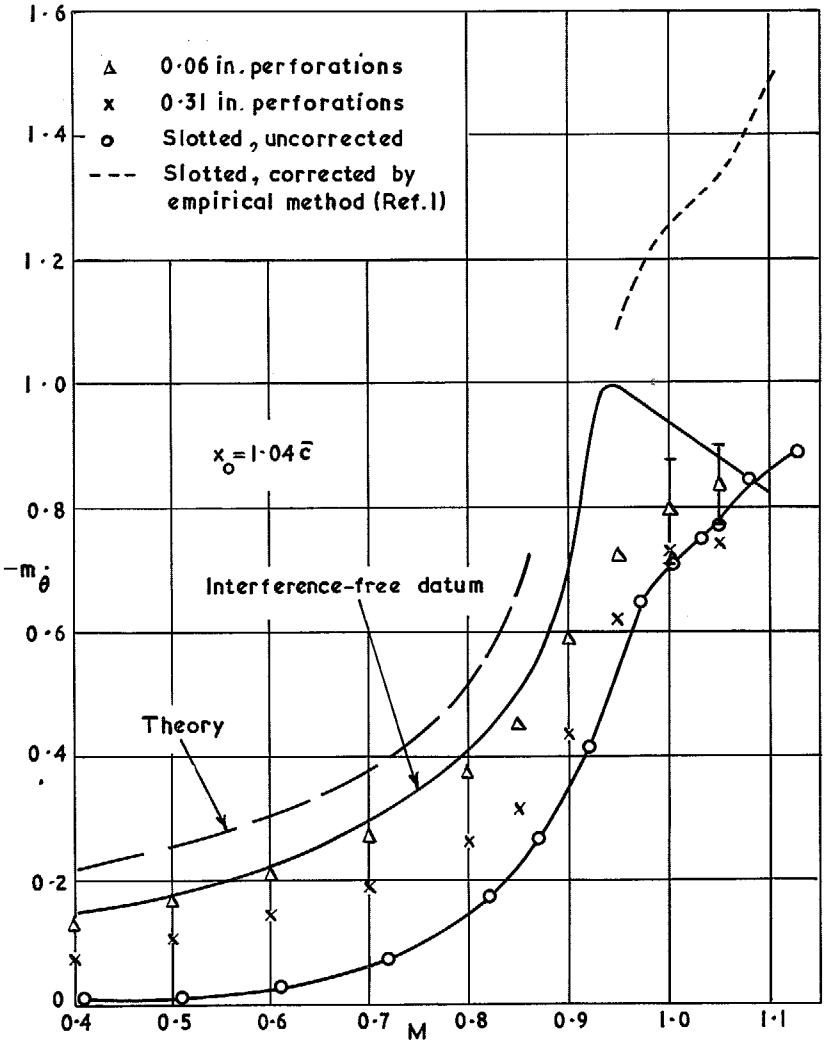

FIG. 8g. Comparison of results from the $9\frac{1}{2}$ in × $9\frac{1}{2}$ in tunnel with interference-free values of pitching damping.

Printed in England for Her Majesty's Stationery Office by the Royal Aircraft Establishment, Farnborough.
Dd. 146916 K5.

Published by
HER MAJESTY'S STATIONERY OFFICE

To be purchased from
49 High Holborn, London WC1
13a Castle Street, Edinburgh EH2 3AR
109 St Mary Street, Cardiff CF1 1JW
Brazennose Street, Manchester M60 8AS
50 Fairfax Street, Bristol BS1 3DE
258 Broad Street, Birmingham 1
7 Linenhall Street, Belfast BT2 8AY
or through any bookseller

R. & M. No. 3636

SBN 11 470336 1